

## Nanonewton force-controlled manipulation of biological cells using a monolithic MEMS microgripper with two-axis force feedback

This article has been downloaded from IOPscience. Please scroll down to see the full text article.

2008 J. Micromech. Microeng. 18 055013

(<http://iopscience.iop.org/0960-1317/18/5/055013>)

View [the table of contents for this issue](#), or go to the [journal homepage](#) for more

Download details:

IP Address: 128.100.48.213

The article was downloaded on 07/10/2010 at 23:31

Please note that [terms and conditions apply](#).

# Nanonewton force-controlled manipulation of biological cells using a monolithic MEMS microgripper with two-axis force feedback

Keekyoung Kim, Xinyu Liu, Yong Zhang and Yu Sun

Advanced Micro and Nanosystems Laboratory, University of Toronto, 5 King's College Road, Toronto, ON M5S 3G8, Canada

E-mail: [sun@mie.utoronto.ca](mailto:sun@mie.utoronto.ca)

Received 24 January 2008, in final form 26 February 2008

Published 1 April 2008

Online at [stacks.iop.org/JMM/18/055013](http://stacks.iop.org/JMM/18/055013)

## Abstract

As mechanical end-effectors, microgrippers enable the pick–transport–place of micrometer-sized objects, such as manipulation and positioning of biological cells in an aqueous environment. This paper reports on a monolithic MEMS-based microgripper with integrated force feedback along two axes and presents the first demonstration of force-controlled micro-grasping at the nanonewton force level. The system manipulates highly deformable biomaterials (porcine interstitial cells) in an aqueous environment using a microgripper that integrates a V-beam electrothermal microactuator and two capacitive force sensors, one for contact detection (force resolution: 38.5 nN) and the other for gripping force measurements (force resolution: 19.9 nN). The MEMS-based microgripper and the force control system experimentally demonstrate the capability of rapid contact detection and reliable force-controlled micrograsping to accommodate variations in size and mechanical properties of objects with a high reproducibility.

(Some figures in this article are in colour only in the electronic version)

## 1. Introduction

Manipulation of micro- and nanometer-sized objects has found important applications in many areas. For instance, automated microrobotic injection of foreign materials into biological cells greatly facilitates the screening of biomolecules and drug compounds [1, 2]. Manipulation of nanomaterials (e.g., carbon nanotubes and nanoparticles) with AFM [3–5] or in scanning electron microscope (SEM) and transmission electron microscope (TEM) [6–8] enhances the capability for nano device construction.

Besides visual feedback from optical or electron microscopes, interaction forces between the end-effector and sample under manipulation represent another important form of feedback. Particularly, many objects to be manipulated, such as biomaterials and microelectromechanical systems (MEMS) components are often fragile and prone to damage, necessitating the detection and control of interaction forces

in order to avoid sample damage. Employing different types of end-effectors and force sensors, several force-controlled micro- and nanomanipulation systems have been reported [5, 9, 10].

In an AFM-based nanomanipulation system [5], a cantilever probe was used as both an end-effector and a force sensor to conduct force-controlled pushing of nanoparticles on a substrate. Microprobe-based three-dimensional manipulation of microspheres was also reported [9], in which a piezoresistive force sensor was integrated to provide force feedback for a proportional-integral (PI) controller. Although pick-and-place of microspheres was demonstrated in the air by virtue of adhesion forces, the operation reliability/reproducibility was low, which is affected by many factors such as sample type and size, temperature and humidity. Moreover, pick-and-place using a single probe is only possible in dry or humid (versus liquid) environments since adhesion forces such as electrostatic force

and surface tension would become less significant in an aqueous environment where biomaterials survive [11].

Compared to micro- and nanoprobes with a single end, a microgripper having two gripping arms permits more reliable and controlled manipulation in both air and liquid. A microassembly system using a piezo-driven meso-scaled gripper was developed to assemble micro-parts into three-dimensional structures [10]. Strain gauges were attached to the gripping arms for gripping force measurements. Although this gripper design has a low force sensing resolution (sub-millinewton), it demonstrated that micrograsping is a viable approach for dexterous micromanipulation tasks. For force-controlled micro- and nanomanipulation, microgrippers should ideally be capable of providing multi-axis force feedback: (1) to protect the microgripper and detect contact between the microgripper and object to be manipulated; and (2) to provide gripping force feedback for achieving secured grasping while protecting the grasped object.

Over the past two decades, continuous efforts have been spent on the design and fabrication of microgrippers based on different mechanical structures and actuation principles [12–20]. Many microgripper designs [12–17] focused on material selection, structure synthesis, microfabrication, actuator design to achieve large output motions and large gripping forces, and applicability to diverse environments. However, these devices commonly do not have integrated force sensors, and thus cannot perform force-controlled micro- and nanomanipulation.

To address this issue, hybrid microgrippers using piezoresistive or piezoelectric force sensors have been demonstrated, where force sensing components were attached to the gripper structures for detecting gripping forces [18, 19]. The force resolution of hybrid microgrippers is relatively low (tens of microNewtons). Furthermore, manual assembly of force sensors can produce misalignments and cause significant errors in force measurement.

In order to construct monolithic microgrippers with a high force sensing resolution, microfabrication was used to produce microgrippers with on-chip actuators and force sensors in a batch manner. Recently reported monolithic microgrippers included an electrostatic microactuator and a single capacitive force sensor for manipulating micro objects [20] and for investigating charge transport of DNA [21]. However, no closed-loop force-controlled micrograsping was demonstrated. The lack of force sensing capabilities along the normal direction for detecting contact forces also makes the microgrippers prone to device breakage during manipulation.

This paper presents the first demonstration of force-controlled micrograsping of biological cells at the nanonewton force level, which is conducted with a monolithic MEMS-based microgripper with integrated two-axis force sensors (figure 1). Biological cells were selected for manipulation due to their high delicacy, high deformability, variations in sizes and mechanical properties among individuals of the same cell line, making them ideal for verifying the effectiveness of the force-controlled manipulation system.

The MEMS-based microgripper employs a V-beam electrothermal actuator for generating grasping motions and

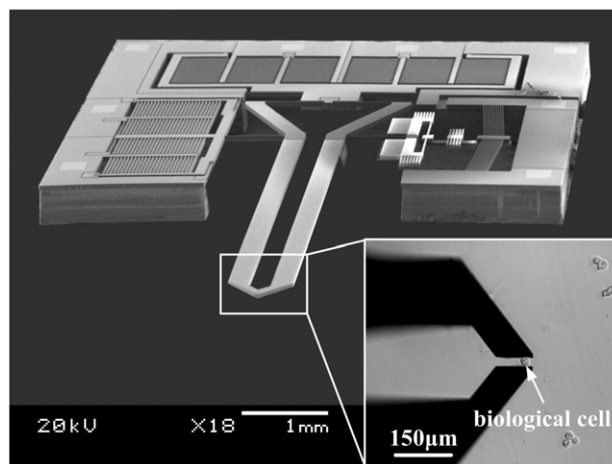


**Figure 1.** MEMS-based microgripper with integrated two-axis force sensor. Inset picture shows nanonewton force-controlled grasping of a biological cell.

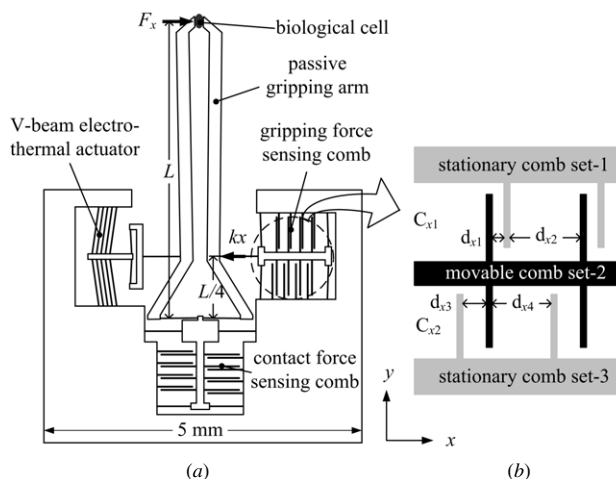


**Figure 2.** Device schematics: (a) microgripper, (b) differential tri-plate comb drive. The schematic shows a deflected situation.

integrates two-axis differential capacitive force sensors for sensing both gripping forces and contact forces between the gripping arm tips and a sample/substrate. Detection of the contact between the substrate and gripping arm tips is achieved with a 39.5 nN force resolution within seconds. A proportional-integral-derivative (PID) force controller is used to regulate gripping forces for force-controlled micrograsping. Experimental results on force-controlled manipulation of micrometer-sized porcine aortic valve interstitial cells (PAVICs) in cell culture medium are presented, demonstrating that the microgripper and control system are capable of performing robust force-controlled micromanipulation at a force level of 20 nN.

## 2. Microgripper design, fabrication and calibration

Figure 2(a) shows a schematic of the microgripper design. A V-beam electrothermal actuator is used to control the opening

of the active gripping arm for object grasping. With an applied voltage, the V-beams are heated and thus, expand to produce motion. The shown microgripper is a commonly closed type with an initial opening of 5  $\mu\text{m}$ . When actuated, the active gripping arm is pulled open. In order to prevent a high temperature at the gripping arm tips, electrical and thermal isolation on the device silicon layer is implemented, and many heat sink beams are used.

Compared to other types of microactuators such as electrostatic [12, 15, 20, 21], piezoelectric [10, 18] and U-beam electrothermal actuators [16, 17], V-beam electrothermal actuators require a much smaller chip area and low driving voltage, produce large forces, and generate large displacements through motion amplification. For the microgrippers reported in this paper, a displacement of 67  $\mu\text{m}$  is produced with an application of 10 V. The much simpler structure of the V-beam actuator (e.g., compared to thousands of comb fingers in electrostatic microgrippers [20, 21]) also significantly helps to increase microfabrication yield.

Integrated capacitive force sensors are implemented with transverse differential comb drives and are orthogonally configured. The force sensors enable the measurement of gripping forces as well as contact forces applied at the end of gripping arms along the normal direction ( $y$  direction in figure 2(a)), both with a resolution of tens of nanonewton. The gripping force sensor permits secured grasping of an object without applying excessive forces; and the normal force sensor is effective to prevent device breakage when the gripping arms approach a substrate.

Four tethering beams are directly connected to the two gripping arms for transmitting forces. A gripping force (along the  $x$  direction) or contact force (along the  $y$  direction), respectively, deflects four unidirectional sensor springs and further changes comb finger gaps. The total capacitance change resolves an applied force. The eight sensor springs are orthogonally configured to decouple force sensing along the  $x$  and  $y$  directions. When a gripping force  $F_x$  is applied to an object (figure 2(a)),

$$F_x L = \frac{kxL}{4}, \quad (1)$$

where  $k$  is the total spring constant of the four sensor springs,  $x$  is the deflection of movable comb fingers and  $L$  is the total length of gripping arms. The four sensor springs are modeled as two fixed-fixed beams with a point load applied in the middle. Thus, the spring constant  $k$  is

$$k = 4 \frac{Et w^3}{l^3}, \quad (2)$$

where  $E = 100$  GPa is the average Young's modulus of P-type (100) silicon, and  $l$ ,  $w$  and  $t$  are spring length, width and thickness.

In order to achieve a high sensitivity and linear input-output relationship, transverse tri-plate differential comb drives shown in figure 2(b) are used [22]. Capacitances are

$$C_{x1} = n \frac{K \varepsilon_0 t l}{d_{x1}} + n \frac{K \varepsilon_0 t l}{d_{x2}}, \quad C_{x2} = n \frac{K \varepsilon_0 t l}{d_{x3}} + n \frac{K \varepsilon_0 t l}{d_{x4}}, \quad (3)$$

where  $K$  is the dielectric constant for air,  $\varepsilon_0$  is the permittivity of free space,  $t \times l$  is the overlapping area of comb fingers and  $n$  is the number of comb finger pairs.

When a gripping force is transmitted to the  $x$  directional force sensor, movable comb set-2 in figure 2(b) moves away from stationary comb set-3 and closer to stationary comb set-1. The gaps between comb fingers become  $d_{x1} = d_0 - x$ ,  $d_{x2} = d'_0 + x$ ,  $d_{x3} = d_0 + x$  and  $d_{x4} = d'_0 - x$ . Capacitance changes are measured by a readout circuit. The corresponding voltage changes are determined as

$$V_{\text{out-}x} = V_{\text{ref}} \left( \frac{C_{x1} - C_{x2}}{C_{x1} + C_{x2}} \right) = V_{\text{ref}} \frac{x d'_0 - x d_0}{d_0 d'_0 - x^2} \cong V_{\text{ref}} \frac{x}{d_0}. \quad (4)$$

By initially setting  $d_0 \ll d'_0$ , the resulting output signal  $V_{\text{out-}x}$  is proportional to the middle-plate displacement,  $x$ . Therefore, the undesired additional capacitive effect can be minimized by placing repeated comb-plate units reasonably far apart (e.g.,  $d_0 = 5$   $\mu\text{m}$  and  $d'_0 = 20$   $\mu\text{m}$  used in this design). In this reported design, when  $x < 2$   $\mu\text{m}$ , input-output linearity is better than 1.5%. The above analysis is also applicable to the  $y$  direction. Structural-electrostatic coupled finite element simulation was conducted to determine spring dimensions and the placement of comb drives to maximize sensitivity while minimizing cross-axis coupling and nonlinearity.

The microgrippers were fabricated with an SOI wafer with a device layer of 50  $\mu\text{m}$  using a process modified from [23] shown in figure 3.

*Step a.* Plasma-enhanced chemical vapor deposition (PECVD)  $\text{SiO}_2$  on the SOI handle layer. Reactive ion etching (RIE) to pattern the PECVD  $\text{SiO}_2$  layer. Deep reactive ion etching (DRIE) for a depth of 100  $\mu\text{m}$ .

*Step b.* RIE to remove  $\text{SiO}_2$ .

*Step c.* DRIE etch until the buried  $\text{SiO}_2$  layer. This two-step DRIE etching creates a step between the central suspended structure and the device frame, which greatly reduces the risk of device breakage during device operation and handling.

*Step d.* HF wet etch to remove buried and deposited  $\text{SiO}_2$ .

*Step e.* E-beam evaporate Al and wet etch to form Al electrodes on the device layer.

*Step f.* Bond the SOI wafer to a support wafer using heat-conductive grease (Cool-grease 7016, AI Technology). DRIE through etch the top device layer to release individual devices.

The microfabrication process and the use of an SOI wafer permit the creation of electrically insulated but mechanically connected structures as well as effective thermal insulation. Microgrippers were wire-bonded to a custom-designed circuit board. The readout circuit was built around an ASIC from Analog Devices (AD7746) for measuring capacitance changes.

Force sensor calibration was conducted using a precision microbalance (XS105DU, Mettler Toledo) with a resolution of 0.1  $\mu\text{N}$ . Figure 4 shows the calibration results of the force sensors along both the  $x$  and  $y$  directions, proving a linear relationship between applied forces and voltage changes (linearity better than 6%) and suppressed cross-axis coupling.

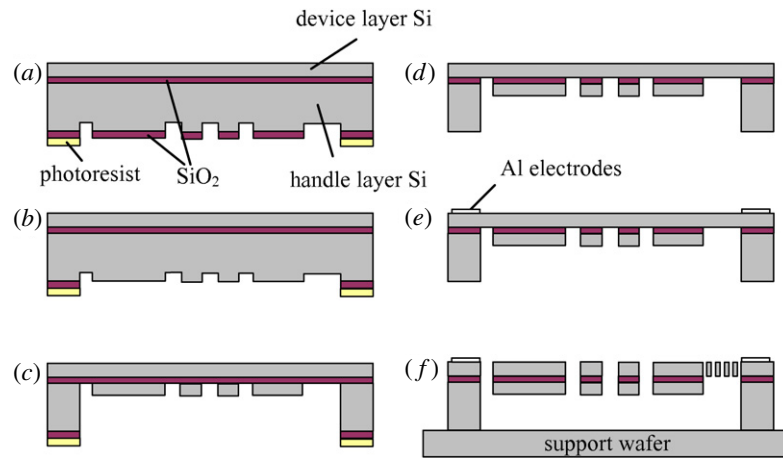


Figure 3. Microgripper fabrication flow.

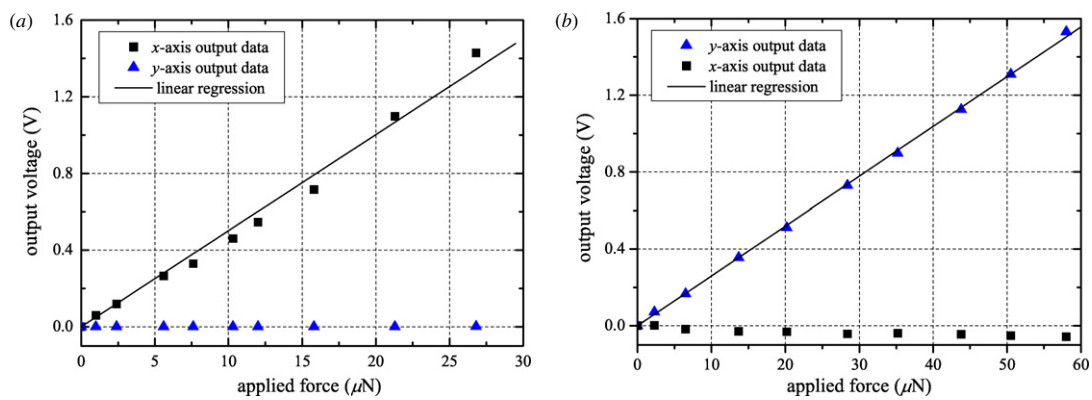


Figure 4. Force sensor calibration results. Forces applied only (a) along the x direction and (b) along the y direction. Also shown are coupled responses.

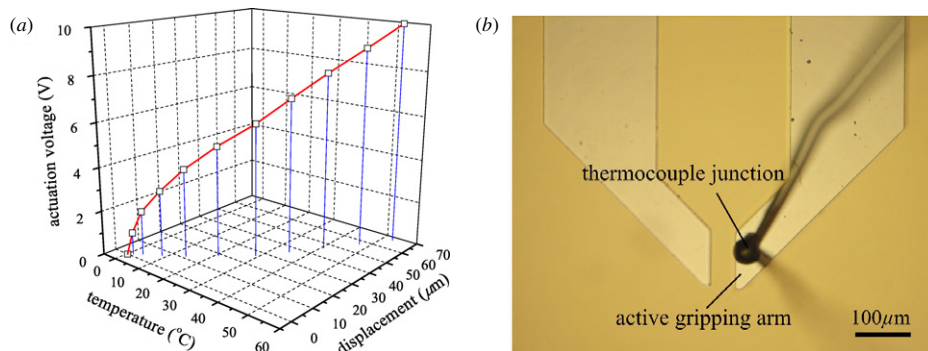
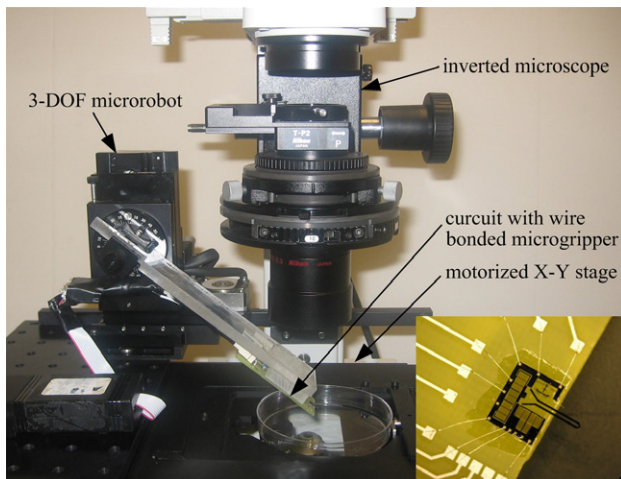


Figure 5. (a) Measured gripping arm tip displacement and temperature at actuation voltages of 1–10 V. (b) A snapshot showing the use of a micrometer-sized thermocouple for temperature measurement.

The devices have a gripping force measurement range of  $\pm 30 \mu\text{N}$  along the x direction and a contact force measurement range of  $\pm 58 \mu\text{N}$  along the y direction. At a sampling frequency of 15 Hz, the devices were calibrated to have a gripping force resolution of 19.9 nN and a contact force resolution of 38.5 nN.

The temperature of the active gripping arm tip was measured using a fine-gauge thermocouple (CHCO-0005,

Omega) with a  $33 \mu\text{m}$  junction in diameter. Every driving voltage was applied for 30 min to ensure no further temperature increase could occur. As shown in figure 5(a), the gripping arm tip moves by  $57 \mu\text{m}$  at 9 V and measured temperature at the gripping arm tip is  $47^\circ\text{C}$  in air. At 6 V, the gripping arm tip is  $32 \mu\text{m}$ , a displacement sufficiently large for manipulating typical cell lines, and the measured temperature at the gripping arm tip is only  $29^\circ\text{C}$  in air. The temperature is



**Figure 6.** Force-controlled micromanipulation setup. Inset picture shows the wire-bonded microgripper.

believed to be even lower when the microgripper operates in cell culture medium. Figure 5(b) shows a snapshot captured from the displacement and temperature measurement process.

### 3. System setup

The micromanipulation system, as shown in figure 6, includes a 3-DOF microrobot (MP-285, Sutter) for positioning the microgripper, a motorized X-Y stage (ProScan II, Prior) for positioning samples, an inverted microscope (TE2000, Nikon) with a CMOS camera (A601f, Basler), a microgripper wire bonded on a circuit board and a control board (6259, National Instruments) mounted on a host computer. The microgripper was tilted with an angle of  $40^\circ$  to enable the gripping arm tips to reach samples on the substrate without immersing the actuator or force sensors into the culture medium. In order to reduce adhesion of cells to the gripping arm tips and thus, facilitate cell release, the microgripper tips were dip coated with 10% SurfaSil siliconizing fluid (Pierce Chemicals) and 90% histological-grade xylenes (Sigma-Aldrich) for 10 s before use. All the components of the system except the host computer are mounted on a vibration isolation table.

### 4. Experimental results and discussion

Aortic valve leaflets were harvested from healthy pig hearts obtained at a local abattoir. After rinsing with antibiotics, each leaflet was treated with collagenase ( $150\text{U mL}^{-1}$ ,  $37^\circ\text{C}$ , 20 min) and the leaflet surfaces were scraped to remove endothelial cells. The leaflets were then minced and digested with collagenase ( $150\text{U mL}^{-1}$ ,  $37^\circ\text{C}$ , 2 h). The interstitial cells were enzymatically isolated, were grown on tissue culture flasks and were kept in an incubator in standard tissue culture medium (DMEM supplemented with 10% FBS and 1% antibiotics). The medium was changed every 2 days, and the cells were passaged when confluent. P2 cells were trypsinized and re-suspended in standard tissue culture medium at  $105\text{ cells mL}^{-1}$  for use in the experiments.

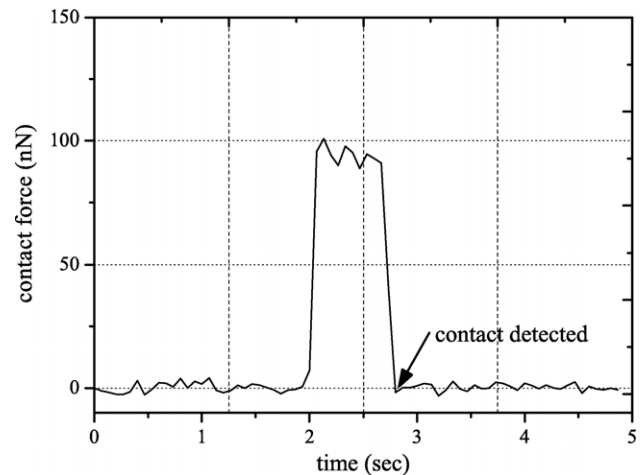


**Figure 7.** Contact force monitoring for reliable contact detection.

The experiments were conducted at room temperature ( $23^\circ\text{C}$ ). A droplet of cell culture medium containing suspended PAVICs (ranging from  $10\text{--}20\ \mu\text{m}$ ) was dispensed through pipetting on a polystyrene petri dish. After PAVICs settled down on the substrate, a microrobot controlled the microgripper to immerse gripping arm tips into the medium droplet. Upon penetration of the droplet, sensing signals rapidly returned to a stable starting level.

#### 4.1. Contact detection

Contact detection is important to protect the microgripper from damage. After the tips of gripping arms are immersed into the medium, the microrobot controls the microgripper at a constant speed of  $20\ \mu\text{m s}^{-1}$  to approach the substrate while force data along the  $y$  direction of the microgripper are sampled. Due to the tilting angle,  $\alpha$  of the microgripper, the  $y$  directional forces,  $F_y$  are converted to contact forces according to  $F_c = F_y \sin(\alpha)$ .

The contact detection process completes within 5 s. Without the integrated contact force sensor, this process would be extremely time consuming and operator skill dependent. When the monitored contact force level reaches a pre-set threshold value, it indicates that contact between the gripping arm tips and the substrate is established. Subsequently, the microrobot stops lowering the microgripper further and moves the microgripper upward until the contact force returns to zero (figure 7). After the initial contact position is detected, the microgripper is positioned a few micrometers above the detected contact position. The pre-set threshold force value used in the experiments was 96 nN, which was effective for reliably determining the initial contact between the gripping arm tips and the substrate.

#### 4.2. Force-controlled grasping of biological cells

Before the system performed force-controlled micrograsping of PAVICs, experiments were conducted to evaluate the effectiveness of open-loop micrograsping. The system applies

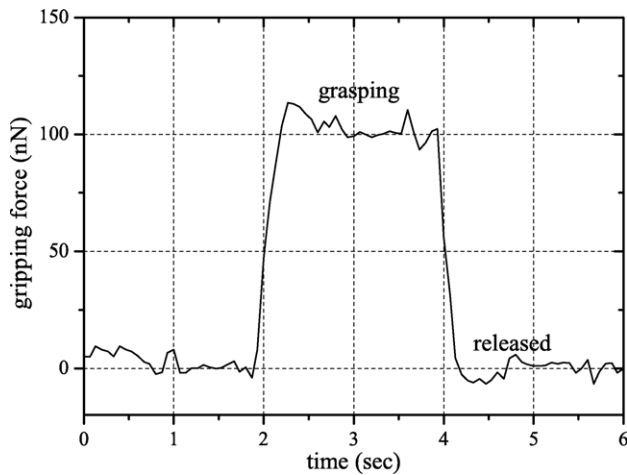


Figure 8. Gripping force profile during micrograsping and releasing of a PAVIC.

a voltage to the V-beam electrothermal actuator to produce an opening larger than the size of a PAVIC between the two gripping arms. When grasping a target PAVIC, the system reduces the applied voltage level, which decreases the arm opening and realizes grasping.

Figure 8 shows the force profile during cell grasping and releasing, where a sequence of actuation voltages was applied

(5 V opening voltage, 3.5 V grasping voltage and 5 V releasing voltage) to grasp and release a 15  $\mu\text{m}$  PAVIC. At 3.5 V grasping voltage, the PAVIC was experiencing a gripping force of 100 nN that produced 15% cell deformation of its diameter. Due to different sizes of PAVICs and their stiffness variations, a single fixed grasping voltage can often cause either unsecured grasping or cell rupturing from excessively applied forces, necessitating closed-loop force-controlled micrograsping.

To achieve reliable micrograsping, a closed-loop control system was implemented by using gripping force signals as feedback to form a closed loop. Figure 9 shows the block diagram of the force control system that accepts a pre-set force level as reference input and employs PID control for force-controlled micrograsping. Figure 10(a) shows the step response of the force-controlled micrograsping system to track a reference input of 100 nN. The settling time is approximately 200 ms. Corresponding to reference input force steps with an increment of 60 nN, tracking results are shown in figure 10(b).

Enabled by the monolithic microgripper with two-axis force feedback, the system demonstrates the capability of rapidly detecting contact, accurately tracking nanonewton gripping forces, and performing reliable force-controlled micrograsping to accommodate size and mechanical property variations of objects. Figure 11 shows three PAVICs of different sizes that were picked, placed and aligned.

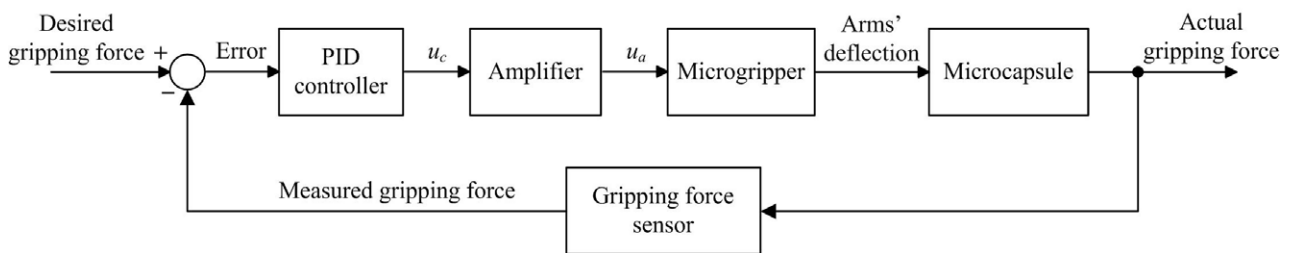


Figure 9. Block diagram of force-controlled micrograsping.

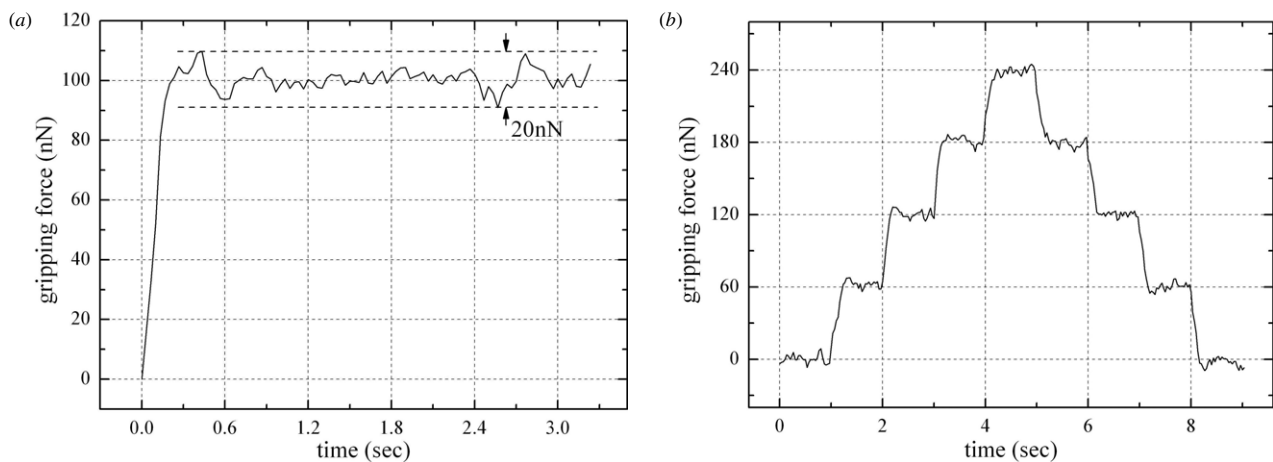
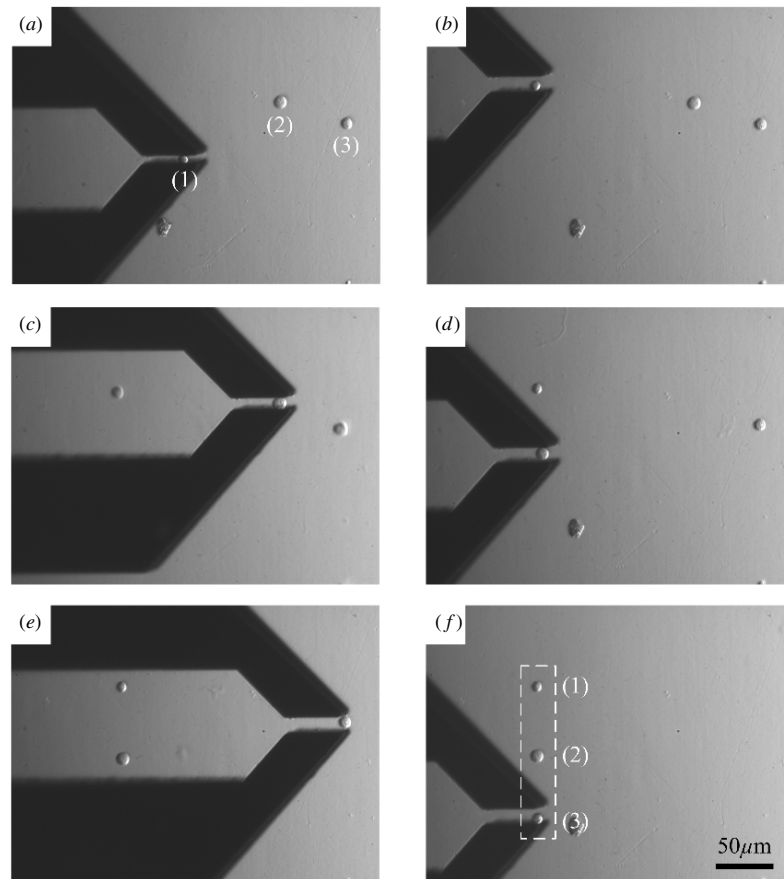


Figure 10. Force-controlled micrograsping. (a) Step response. (b) Tracking force steps with an increment of 60 nN.



**Figure 11.** Cell manipulation and alignment with force-controlled micrograsping. (a) After contact detection, the microgripper grasps a first cell. (b) The microgripper transfers the cell to a new position and releases the cell. (c) The microgripper grasps a second cell. (d) Transferring and releasing the second cell. (e) The microgripper approaches a third cell. (f) Transferring and releasing the third cell. Three cells of different sizes are transferred to desired positions and aligned.

Force-controlled micrograsping of the aligned PAVICs was conducted at a force level of 65 nN.

## 5. Conclusion

This paper demonstrated force-controlled micrograsping of highly deformable PAVICs at a 20 nN force level. The contact force feedback of the MEMS-based microgripper enables the micromanipulation system to conduct rapid contact detection at a nanonewton force level and protects the microgripper from breakage. The gripping force feedback of the microgripper permits force-controlled micrograsping with a PID force controller to accommodate size and stiffness variations of objects to achieve secured grasping with no excessive forces applied. The temperature rise at the gripping arm tips caused by the integrated electrothermal microactuator was determined to be tolerable by biological cells. Besides force-controlled micromanipulation of biomaterials in liquid, the monolithic microgrippers with two-axis nanonewton force feedback can also find important applications in biomaterial mechanical characterization and in electronic component handling as well as the assembly of micro objects.

## Acknowledgments

This work was supported by the Natural Sciences and Engineering Research Council of Canada and by the Ontario Ministry of Research and Innovation. The authors thank Professor C Simmons' group for assistance with interstitial cell preparation.

## References

- [1] Sun Y and Nelson B J 2002 Biological cell injection using an autonomous microrobotic system *Int. J. Robot. Res.* **21** 861–8
- [2] Wang W H, Liu X Y, Gelinis D, Ciruna B and Sun Y 2007 A fully automated robotic system for microinjection of zebrafish embryos *PLoS ONE* **2** e862
- [3] Requicha A A G 2003 Nanorobots, NEMS, and nanoassembly *Proc. IEEE* **91** 1922–33
- [4] Chen H P, Xi N and Li G Y 2006 CAD-guided automated nanoassembly using atomic force microscopy-based nonrobotics *IEEE Trans. Auto. Sci. Eng.* **3** 208–17
- [5] Sitti M and Hashimoto H 2000 Controlled pushing of nanoparticles: modeling and experiments *IEEE Trans. Mech.* **5** 199–211
- [6] Dong L X, Tao X Y, Zhang L, Zhang X B and Nelson B J 2007 Nanorobotic spot welding: controlled metal

- deposition with attogram precision from copper-filled carbon nanotubes *Nano Lett.* **7** 58–69
- [7] Fukuda T, Arai F and Dong L 2003 Assembly of nanodevices with carbon nanotubes through nanorobotic manipulations *Proc. IEEE* **91** 1803–18
- [8] Fatikow S, Wich T, Hulsen H, Sievers T and Jahnisch M 2007 Microrobot system for automatic nanohanding inside a scanning electron microscope *IEEE/ASME Trans. Mech.* **12** 244–52
- [9] Gorman J J and Dagalakis N G 2006 Probe-based micro-scale manipulation and assembly using force feedback *Proc. 1st Joint Emer. Prep. Response/Robotic Remote Sys. Top. Mtg. (Salt Lake City, UT, US)* pp 621–8
- [10] Thompson J A and Fearing R S 2001 Automating microassembly with ortho-tweezers and force sensing *Proc. IEEE/RSJ Int. Conf. Intell. Robot. Syst. (Maui, HI, US)* pp 1327–34
- [11] Fearing R S 1995 Survey of sticking effects for micro parts handling *Proc. IEEE/RSJ Int. Conf. Intell. Robot. Syst. (Pittsburgh, PA, US)* pp 212–7
- [12] Kim C-J, Pisano A P and Muller R 1992 Silicon-processed overhanging microgripper *J. Microelectromech. Syst.* **1** 31–6
- [13] Chu W H and Mehregany M 1994 Microfabrication of tweezers with large gripping forces and a large range of motion *Proc. Solid-State Sensor and Actuator Workshop* pp 107–10
- [14] Kohl M, Just E, Pflöging W and Miyazaki S 2000 SMA microgripper with integrated antagonism *Sensors Actuators A* **83** 1–3
- [15] Millet O, Bernardoni P, Rgnier S, Bidaud P, Tsitsiris E, Collard D and Buchaillot L 2004 Electrostatic actuated micro gripper using an amplification mechanism *Sensors Actuators A* **114** 371–8
- [16] Ivanova K, Ivanov T, Badar A, Volland B E, Rangelow I W, Andrijasevic D, Fischer F S S, Brenner M S W and Kostic I 2006 Thermally driven microgripper as a tool for micro assembly *Microelectron. Eng.* **83** 1393–5
- [17] Chronis N and Lee L P 2005 Electrothermally activated SU-8 microgripper for single cell manipulation in solution *J. Microelectromech. Syst.* **14** 857–63
- [18] Carrozza M C, Eisinger A, Menciassi A, Campolo D, Micera S and Dario P 2000 Towards a force-controlled microgripper for assembling biomedical microdevices *J. Micromech. Microeng.* **10** 271–6
- [19] Kim D H, Lee M G, Kim B and Sun Y 2006 A superelastic alloy microgripper with embedded electromagnetic actuators and piezoelectric force sensors: a numerical and experimental study *Smart Mater. Struct.* **3** 208–17
- [20] Beyeler F, Neild A, Oberti S, Bell D J, Sun Y, Dual J and Nelson B J 2007 Monolithically fabricated microgripper with integrated force sensor for manipulating microobjects and biological cells aligned in an ultrasonic field *J. Microelectromech. Syst.* **16** 7–15
- [21] Yamahata C, Collard D, Takekawa T, Kumemura M, Hashiguchi G and Fujita H 2008 Humidity dependence of charge transport through DNA revealed by silicon-based nanotweezers manipulation *Biophys. J.* **94** 63–70
- [22] Sun Y, Fry S N, Potasek D P, Bell D J and Nelson B J 2005 Characterizing fruit fly flight behavior using a microforce sensor with a new comb drive configuration *J. Microelectromech. Syst.* **14** 4–11
- [23] Sun Y, Nelson B J, Potasek D P and Enikov E 2002 A bulk microfabricated multi-axis capacitive cellular force sensor using transverse comb drives *J. Micromech. Microeng.* **12** 832–40